INTERNATIONAL JOURNAL OF
ENERGY RESEARCH

INTERNATIONAL JOURNAL OF ENERGY RESEARCH
Int. J. Energy Res. 2017; **41**:1202–1210
Published online 20 January 2017 in Wiley Online Library (wileyonlinelibrary.com). DOI: 10.1002/er.3704

Improved electrochemical performance of a cyclic ultracapacitor using slurry electrodes under various flow conditions

Dong-Ha Kim[1,2], Sang-Ho Lee[1], Se-Kook Park[1], Min-Jung Choi[1], Kyoung-Hee Shin[1], Chang-Su Jin[1], Yun Jung Lee[2] and Sun-Hwa Yeon[1,*,†]

[1]Energy Storage Lab., Korea Institute of Energy Research, 102 Gajeong-ro, Yuseong, Daejeon, 305-343, Korea
[2]Department of Energy Engineering, Hanyang University, 222 Wangsimni-ro, Seongdong-gu, Seoul 133-791, Korea

SUMMARY

A cyclic ultracapacitor is a promising energy storage device that can be used for grid energy storage. The cyclic ultracapacitor combines the advantages of both ultracapacitors and flow batteries, enabling rapid charging and large-scale energy use. To improve the electrochemical performance under the flow condition, it is necessary to find a more electrical active material and design a flow cell that minimizes the resistance. In this study, we investigate the effects of changing the ratio of the active material in a slurry electrode under various operating conditions. Slurry electrodes were prepared with different ratios of active material and conductive additive but with a fixed electrolyte amount. Voltage–time curves of both a single and a stack-flow cell in the constant-current mode were obtained to analyze the relationship between the active materials ratio and the cell performance. Having more adsorption sites according to the active material amount is more important than increasing the electric conductivity by the conductive additive amount with regard to cell performance capabilities in a low resistance condition such as a non-flow mode. However, higher electrical conductivity on a slurry electrode is more beneficial to improve the electrochemical performance in the stack-flow mode, which has harsh resistance levels. Copyright © 2017 John Wiley & Sons, Ltd.

KEY WORDS
slurry electrode; conductive additive; stack system; ultracapacitor

Correspondence
*Sun-Hwa Yeon, Energy Storage Lab., Korea Institute of Energy Research, 102 Gajeong-ro, Yuseong, Daejeon 305-343, Korea.
†E-mail: ys93@kier.re.kr

Received 18 August 2016; Revised 24 November 2016; Accepted 1 December 2016

1. INTRODUCTION

The exhaustion of fossil fuels such as coal and oil has led to the search for and improvement of renewable power sources. As a result, renewable energy sources are now being used in various industrial fields, but these sources are intermittent and often unpredictable [1]. Because of the weaknesses of renewable energy sources, the necessity of energy storage systems (henceforth ESS) has come to the fore. Among ESS, electrochemical ESS are much better suited than other devices to meet the required conditions of energy storage devices for renewable energy sources [2,3]. Unlike static and solid batteries, flow batteries allow control of the capacity and energy characteristics, as capacities in this case are influenced by the type of electrolyte and the size of the electrode reservoir used. Hence, redox flow battery can meet the specific requirements of a local energy grid system, a wind plant, or a community block [4]. However, several chronic problems preventing their commercialization have yet to be solved, including cost reductions, long life spans and making the system more compact [5].

Ultracapacitors based on electrochemical double-layer capacitance are another promising electrical ESS owing to their specific advantages, such as a long life span, low cost, reliable stability, fast response, and high power density. They have long been used in many industries, but their short usage times due to their low energy density levels clearly represent limitations when used as an ESS component in renewable energy plants. Although the energy density of ultracapacitors is much higher than that of electrostatic and electrolytic capacitors, it is still lower than that of batteries and fuel cells [6]. Thus, investigations to improve the energy density of ultracapacitors are required before they can be applied to additional devices. As part of the effort to overcome the low energy density

limitation, the new concept of intergrating an ultracapacitor and a flow battery system has recently been developed [7,8]. This new dynamic energy storage device known as an electrochemical flow capacitor (EFC) utilizes a systemic approach beyond merely finding new porous materials to improve the energy density of ultracapacitors [9,10]. The combined use of an ultracapacitor and a battery is necessary for grid energy storage. Given that the EFC has the advantages of both devices, it is practical when applied to large-scale energy storage systems. It is also inexpensive, powerful, reliable, and environmentally friendly [11]. The EFC system is composed of an electrochemical flow cell and four slurry tanks to store the charged and discharged slurries that flow intermittently. One issue with this system is that it reaches the target charge and discharge voltage levels in typical constant-current mode. Because EFCs operate under an intermittent flow condition dependent on time, all slurries in the tank charge up to the target voltage. Hence, the voltage and time curves of flow capacitors in the constant-current mode remain relatively unknown worldwide [12]. The cyclic ultracapacitor (CUCap), introduced in an earlier work [5], consists of a flat flow capacitor cell and two reservoirs. This system can be operated in the cyclic mode for non-intermittent flows, and the power rating and energy capacity levels, as well as the volumes of the slurry reservoirs, can all be independently adjusted. The CUCap system enables the charge and discharge of the target voltage in the constant-current mode under a flow condition, as all slurry electrodes in the reservoir constantly flow in the cell [5]. Generally, both the EFC and CUCap remain limited when used in high-current-density operations ($>10\,mA\,cm^{-2}$) in a large-scale system, as they undergo a shunt current and considerable resistance caused by mass transfers. To overcome these problems, improvements of the cell design and slurry electrode are necessary [13]. Generally, an 'electrochemical flow capacitor' or a 'cyclic ultracapacitor' implies capacitor based on a flowable electrode. Previous studies have attempted to overcome the low energy density that impedes commercialization of supercapacitors. In order to deal with this limitation, various studies have been carries out including the application of activated carbon (AC), pseudocapacitive, and wrapping of active materials and graphene. Furthermore, research to approach the capacitor as large-scale energy storage device through scale up process along with increasing the energy density has been carried out.

In this study, we demonstrate the optimal composition of slurry electrode materials in a CUCap consisting of an active material and a conductive additive (CA) at a constant electrolyte ratio with a new cell design with lower cell resistance levels. The CUCap was tested under three operational modes, the non-flow mode, the flow mode, and stack-flow mode, while varying the slurry electrode viscosities. The electrochemical performance capabilities of the CUCap cell under these operating conditions were found to differ. In the non-flow cell, the cell with 10 wt% CA ($5.1\,Wh\,L^{-1}$ at current density $10\,mA\,cm^{-2}$) showed the highest energy density. However, in the single-flow cell, the best performance was obtained at 30 wt% CA in a flowable electrode (at a slurry ratio of 1 to 7), resulting in volumetric capacitance and energy efficiency values of $8.7\,F\,mL^{-1}$ and 50%, respectively. The highest power was observed at 50 wt% CA in the stack-flow condition. These results lend insight into the optimal system operation of flowing energy storage devices with regard to the optimal electrochemical and rheological properties to obtain high capacity though low resistance in a large-scale system.

2. EXPERIMENTAL

2.1. Electrode preparation

The slurry electrodes consist of porous carbon as an active material (BEAPS-AC0830 (AC), Asahi Organic Chemicals Co., Ltd, Japan), a CA (Super-P, Imerys Graphite & Carbon, Switzerland), and an electrolyte (1.0 M TEABF4 in Acetonitrile, Panaxetec, Republic of Korea) [5]. Before mixing the active material and the electrolyte, powders of the active materials were mixed by ball-milling for 10 h. Active materials at specific ratios were prepared. The CA contents in the powders were 10, 20, 30, 40, and 50 wt%. Following the powder mixing step, each powder was mixed with the electrolyte by ball-milling for 10 h. The electrolyte portions were fixed at 1 to 6 (14.2 wt%).

2.2. Unit cell preparation

Each of the flow cells has similar components to impart the properties of a CUCap device. All cells have in common two graphite electrodes, steel use stainless current collectors, poly-tetra-fluoro-ethylene (PTFE) frames intagliated channels, and PTFE gaskets, but the stack-flow cell has more graphite electrodes, channels, and gaskets than the single-flow cell. The PTFE frame of the channel depth was designed with an additional difference to ensure a smooth flow. The frame for a non-flow cell has a channel depth of only 500 μm, whereas the others have channel depths of 1500 μm. The flat cell was designed with an octahedral shape, and the area was $78\,cm^2$. Both the flow cell and the stack-flow cell have the same experiment conditions for the pump and tubing. The pumps (Masterflex no. 7523-80) to inject the flowable electrode in the flow cell, which can adjust flux per time, are positioned at both sides of the flow cell. The tubing material is Norprene, which has high durability and chemical resistance. The pump speed is $200\,mL\,min^{-1}$ which provided the best performance in our recent research [5].

2.3. Electrochemical measurements

Electrochemical measurements were conducted at room temperature with a potentiostat/galvanostat (Battery Cell Charge/Discharge Test System, MACCOR Series 4000). Galvanostatic charging/discharging was carried out at

different current densities according to the operating conditions of each cell. Non-flow cells showed high current density (from 5 to 200 mA cm^{-2}) and voltage cutoff of 2.7 V. However, the single-flow cell was operated at a low current density and at identical voltage levels (10, 20, and 30 mA cm^{-2} and from 0 to 2.7 V, respectively). The two-stack flow system used the same current density but different voltages compared with the single-flow cell. Electrochemical impedance spectroscopy tests were conducted at ambient temperatures with a potentiostat/gavanostat (Autolab PGSTAT30) accomplished with a FRA32M frequency response analyzer module. The electrochemical impedance spectroscopy test conditions included the open circuit voltage, a 5 mV amplitude, and a frequency range from 200,000 to 0.01 Hz. The specific capacitance, *Csp*, was calculated via galvanostatic cycling using Eq. (1),

$$Csp = \frac{2i}{m \cdot \left(\frac{dV}{dt}\right)}. \quad (1)$$

where i is the discharge current and dV/dt is the slope of the discharge curve. The energy efficiency was calculated using Eq. (2):

$$E_{eff} = \frac{\int I_{discharge} v_{discharge} dt}{\int I_{charge} v_{charge} dt} \times 100 \quad (2)$$

The energy density was calculated as follows (Eq. (3)):

$$E = \frac{1}{2v} CV^2 \quad (3)$$

where C is the capacitance of the unit cell, V is the discharge voltage, and v is the volume of the slurry electrodes. The power of the stack cell was calculated with Eq. (4)

$$P = V_{net} I \quad (4)$$

where I is the discharge current and V is net discharge voltage excluding the IR drop (Ohmic drop). The resistance of stack cell was calculated using Eq. (5):

$$R = \frac{V_{ir\ drop}}{I} \quad (5)$$

Here, *Virdrop* denotes the discharge voltage, and I is the discharge current [3].

2.4. Morphological observation

Cryo-scanning electron microscopy (Cryo-SEM) images of the slurry electrodes were obtained using a Tescan Mira 3 LMU FEG instrument (Tescan, Czech Republic) that was prepared with a Quorum Technologies PP300T Cryo-SEM sample preparation system. The accelerating voltage, sublimation condition, and coating condition were 10 kV, −100 °C for 10 min, and 10 mA and 120 s Pt

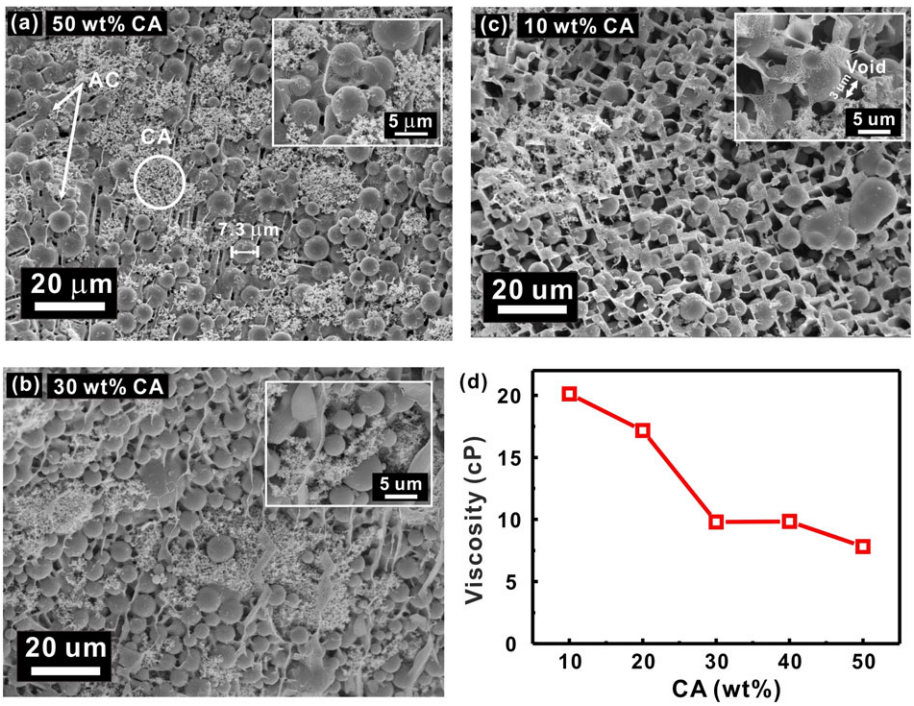

Figure 1. Cryo-scanning electron microscopy images of slurries with different ratios of activated carbon and a conductive additive (the conductive additive ratio: (a) 50 wt%, (b) 30 wt%, (c) 10 wt%). Each activated carbon sample has networks created by the dispersing conductive additive. The images show the state of the electrode at the moment of the flow through the channel. (d) Viscosities of the slurry electrodes with variation of conductive additives quantities. AC, activated carbon; CA, conductive additive. [Colour figure can be viewed at wileyonlinelibrary.com]

Int. J. Energy Res. 2017; **41**:1202–1210 © 2017 John Wiley & Sons, Ltd.
DOI: 10.1002/er

coating, respectively. The slurry samples were prepared in each set of conditions, and the recipes were identical to those used to prepare the electrodes.

3. RESULTS AND DISCUSSION

Figure 1 shows cryo-SEM images of a slurry electrode composed of the active materials (AC, AC0830) and the organic electrolyte at a ratio of 14.2 wt%. The active material powders had different ratios of CAs with 50 wt% (Figure 1(c)) of AC spheres. This cryo-SEM technique can be useful in that the mixing state and morphology of the carbon spheres and the nano-CA in the liquid electrolyte can be observed according to the increase of the viscosity in the slurry state. For the cryo-SEM process, the samples were loaded onto a cryo-specimen holder and cryo-fixed in a nitrogen slush (−210 °C), after which they were quickly transferred to the cryo unit in a frozen state. The frozen samples were then fractured by striking them with a pre-cooled razor blade at a certain point on the surface established as the fracture plane. The revealed fracture plane was sublimed at −85 °C in a vacuum SEM chamber and then examined by cryo-state SEM. The AC, with a uniformly spherical size of approximately 7 μm, was mixed with a nano-sized, spherical CA. In the three samples of Figure 1(a), (b), and (c), aggregation of the CA is apparent between the active carbon particles with an increase in the weight portion of the additive. In the case of the slurry electrode with 10 wt% CA, a few inter-voids (distance, 1 ~ 2 μm distance) between the spherical carbon particles are shown because of the greater amount of active carbon as compared with the other additive portions, in this case the 30 and 50 wt% samples.

The electrochemical properties are closely related to the electrode rheology, which can be affected by the composition of the slurry electrode, including the active carbon, CA, and electrolyte. Figure 1(d) shows the viscosities of the slurry electrodes with the variation of the amount CAs. The viscosities have a tendency to decrease according to an increase of the CA ratio. This tendency has a huge influence on the resistance under a flow condition. We anticipate that in flow mode, low viscosity of the slurry electrode would facilitate system operation because of its high fluidity, thereby improving the electrochemical performance. The carbon particles, particle size/shape, and carrier-fluid electrolyte have significant effects on the performance capabilities of the slurry electrodes. In previous work, a spherical carbon with a narrow particle size distribution was recommended for rheological advantages

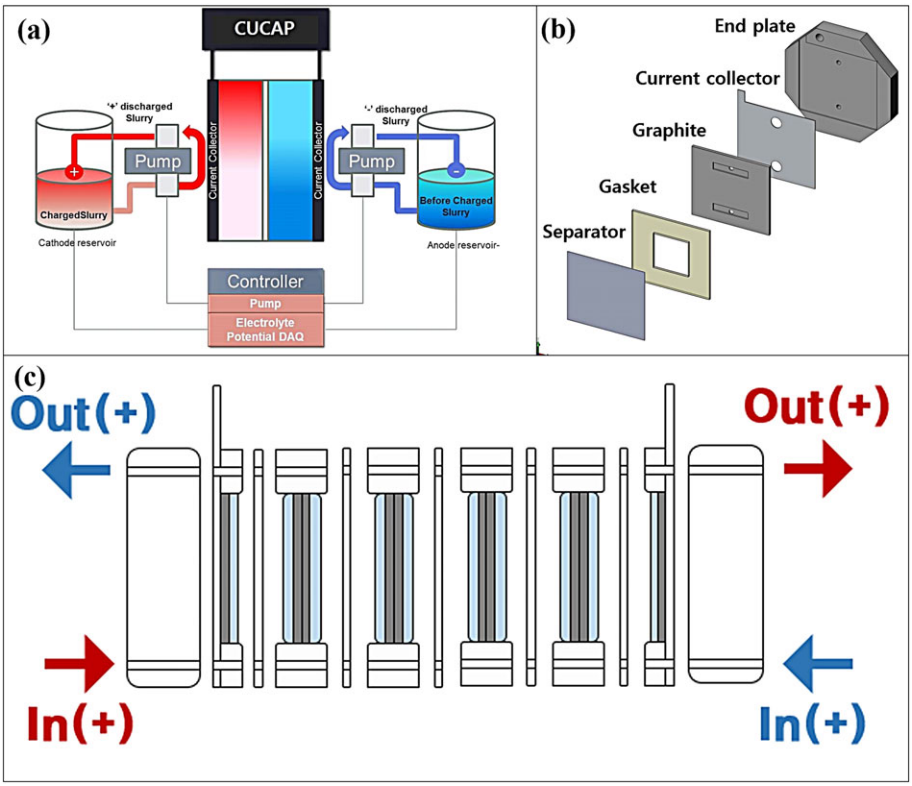

Figure 2. (a) Schematic of the operation system of a cyclic ultracapacitor (CUCap) sample positioned in a symmetric flow channel and the tank containing (+)-charged and (−)-charged slurries. (b) A plot of a single cell showing the assembly sequence, and (c) isometric drawing of the stack-flow system in which anodic and cathodic electrodes are individually flowing in the flow channel. [Colour figure can be viewed at wileyonlinelibrary.com]

in that this type of carbon minimized flow-induced particle size segregation and clogging [3]. The slurry was prepared by mixing carbon with carbon black to achieve a 9:1 weight ratio. The carbon black was used as a CA. In this study, while the composition of the AC and CA under flowing and non-flowing states was achieved at a ratio of 14.2 wt% of the electrode to the electrolyte, composition of the CA was varied to assess the influence of these changes on the rheology and electrochemical properties. By increasing the CA mass ratio from 10 to 30 and 50 wt%, the slurry was observed to exhibit improved macroscopic flow capabilities.

Figure 2 shows schematic diagrams of (i) the CUCap charge/discharge system, (ii) a single-flow cell, and (iii) the flow sequence in the stack-flow cell system. Cathodic and adodic slurries in the reservoir are injected into the electrode area and are charged by cathodic and anodic current, respectively. The slurries injected by a pump into the flow cell were charged gradually, after which each was charged with different corresponding ions stored in the reservoir. Over time, the voltages of the slurries in both the reservoir and the flow cell increased steadily in the slurry flow state. When the target voltage was reached, fully charged slurries resulted to the extent of, the reservoir tank size and the amount of energy that could be stored, as shown in Figure 2(a). If the volume of the slurry reservoirs doubles, the discharge time doubles as well. To discharge the slurries, discharge current can simply be applied using an identical procedure. Figure 2(b) shows that the single-flow cell is assembled with two graphite electrodes, steel use stainless current collectors, PTFE gaskets, polyvinyl chloride end frames, and a symmetrical separator toward the center. The two-stack flow cell shown in Figure 2(c) has a similar structure as compared with the single-flow cell. It has more components than the single-flow cell, such as a pair of electrodes, current collectors, gaskets, and one separator. The number of stacked cells is equal to the number of separators. The stacked-cell system should be carefully assembled because of the possibility self-discharge. If any of the charged slurry and graphite components come into contact in the cell or channel, the voltage increase can be stopped by the resulting shunt current.

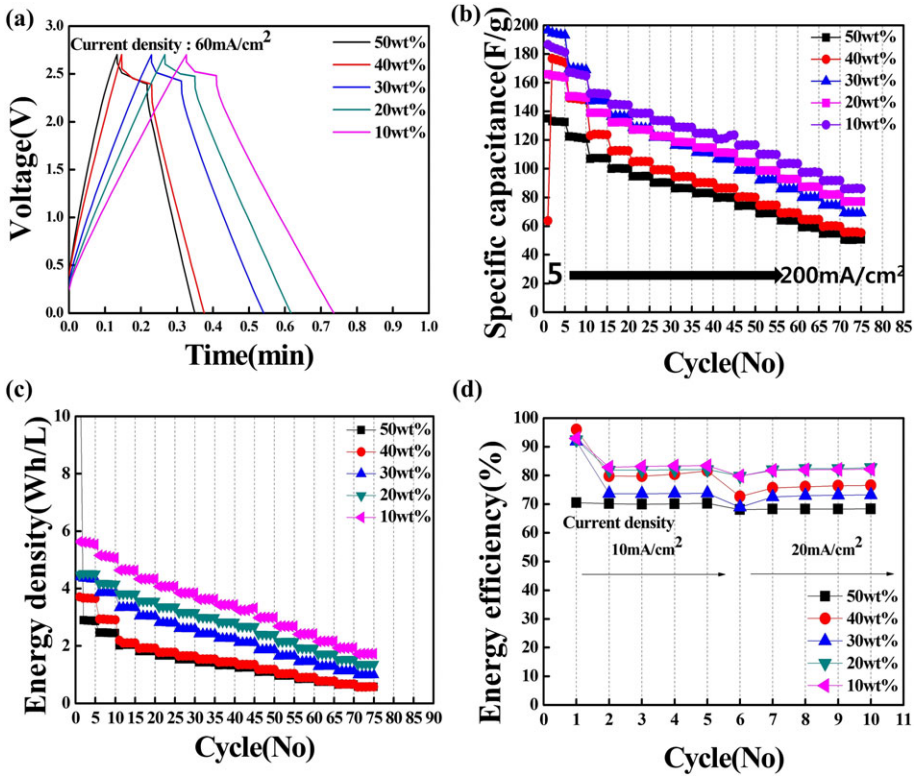

Figure 3. Voltage–time curves of each ratio of conductive additives were investigated using a constant-current method. Slurries containing activated carbon (AC0830) and conductive additives (SUPER-P) were charged from 0 to 2.7 V at a current density of 60 mA cm^{-2}. (a) The quantitative parameters of a slurry electrode using organic electrolyte (1 M TEABF4 in acetonitrile) and activated materials, at different ratios, as tested to investigate the cell performance capabilities. The current density ranges from 10 to 200 mA cm^{-2}, and five cycles each with a gap of a gap of 10 mA cm^{-2} were used. (The data in this figure were obtained under a non-flow condition.). (b) Specific capacitances of the active materials excluding the electrolyte weight, (c) energy density when substituting the carbon weight for the slurry weights, and (d) energy efficiency at low current density levels (10 and 20 mA cm^{-2}). [Colour figure can be viewed at wileyonlinelibrary.com]

Int. J. Energy Res. 2017; **41**:1202–1210 © 2017 John Wiley & Sons, Ltd.
DOI: 10.1002/er

Figure 3 shows the electrochemical performance of the non-flow cell at step-current density levels of 5–200 mA cm^{-2} (five cycles each). The cell voltages were swept from 0 to 2.7 V when using the slurry electrode with a 1 to 7 ratio of the electrode (AC + (CA)) electrolyte (1 M TEABF4 in acetonitrile). The voltage profile of the non-flow cell at a current density of 60 mA cm^{-2} according to the CA ratio shows that the charge/discharge time of a cell containing 10 wt% of a CA is longer than any of others, as shown in Figure 3(a). This is why the cell containing 10 wt% CA has more AC, giving it more sites for ion adsorption. However, each cell displays a tendency such that the charge/discharge time of a cell with a small amount of AC decreases gradually. Also, we can show nonlinear behavior between charge and discharge curves because of step time to measure the resistance and IR drop. Figure 3(b) shows that the cells containing 10 wt% CA and 30 wt% CA exhibit specific capacitance levels of 187 and 195 at 5 mA cm^{-2}, respectively. The slurry electrode containing 30 wt% CA exhibits the highest capacitance among the non-flow cells. However, once the current density increases, the specific capacitance of the 30 wt% CA case decreases more rapidly compared with that of the 10 wt% CA case. While the specific capacitances of the 30 wt% CA at 10, 20, 30, 40, and 50 mA cm^{-2} samples are 173, 155, 143, 139, and 131 F g^{-1}, respectively, and the specific capacitances of the 10 wt% CA at 10, 20, 30, 40, and 50 mA cm^{-2} samples are correspondingly 171, 158, 153, 149, and 145 F g^{-1}. We found that the specific capacitance was influenced by the ratio of the active materials from 20 mA cm^{-2}, as shown in Figure 3(b). Figure 3(c) shows that energy density of the cell containing 10 wt% CA exhibits the highest value, 5.8 Wh kg^{-1}, among the CA conditions. As shown in Figure 3(a), the net discharge voltages are similar in all cells. Therefore, the parameter determining the energy density is the specific capacitance, as shown in the unit cell. We can determine the energy density of the cell using an equation that takes into account the net discharge voltage and the unit cell capacitance, as shown in Figure 3(c). The energy efficiency in an energy storage device is the most important parameter evaluating electrochemical properties. The energy efficiency of cell containing 10 wt% CA was 82.7% at 10 mA cm^{-2} and 81.6% at 20 mA cm^{-2} under a non-flowing condition, as shown in Figure 3(d).

Figure 4 shows the charge/discharge voltage profiles, the volumetric specific capacitance levels, and the energy efficiency capabilities from the CUCap under a flowing condition in a single cell. We found that the electrochemical capacities show lower values than those in the non-flowing condition due to mass transfer resistance under the flowing condition. In the voltage profile shown in Figure 4(a), the flow cell containing 50 wt% CA and the flow cell containing 10 wt% CA have a high net discharge voltage (a low IR drop) and a low net discharge voltage (high IR drop), respectively. The flow cell containing 30 wt% CA is positioned in the middle in this case, as shown in the time–voltage curve in Figure 4(a), but the discharge time is longer. At this point, the flow cell containing 30 wt% CA shows the highest specific volumetric capacitance, as shown in Figure 4(b). Figure 4(c) shows

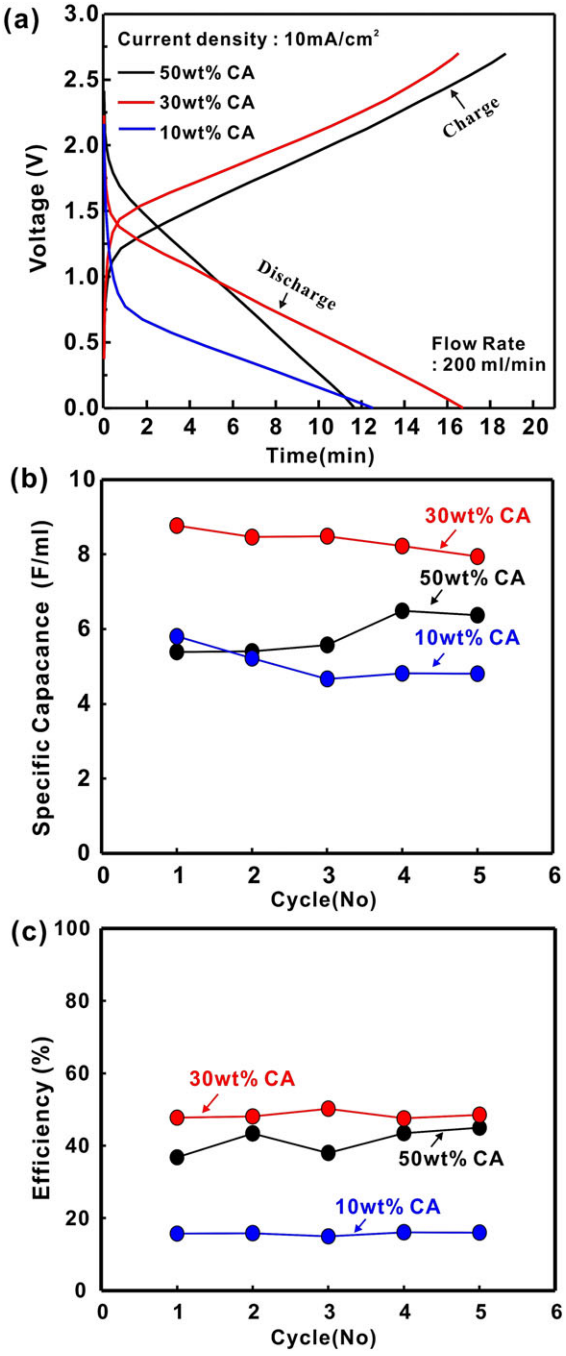

Figure 4. The electrochemical performance of a CUCap (single-flow cell) sample using according to the galvanostatic charge/discharge methods: (a) voltage–time curves, (b) volumetric capacitance, and (c) energy efficiency comparison with each ratio of active materials under identical conditions (current density at 10 mA cm^{-2}, flow rate of slurry electrode = 200 mL min^{-1}, the volume of slurry reservoir = 150 mL (each one at 75 mL)). CA, conductive additive. [Colour figure can be viewed at wileyonlinelibrary.com]

that the flow cells containing 30, 50, and 10 wt% CA exhibit specific capacitances 8.7, 6.3, and 4.5 F mL^{-1}, respectively. The 10 wt% cell has a high discharge slope but a low specific capacitance due to its harsh IR drop. This trend becomes severe in terms of energy efficiency. The flow cells containing 30, 50, and 10 wt% CA show energy efficiency values of 50%, 40%, and 18%, respectively.

Figure 5 shows the electrochemical performance related to the power in the two-stack flow condition in the CA 50, 30, and 10 wt% cells. In the voltage–time curve in Figure 5 (a), the discharge times and charge/discharge slopes clearly change according to the ratio of the active materials because of the different electric conductivities in the slurry electrodes. The cell containing 50 wt% CA has the longest discharge time among the samples, with a gradual discharge slope. When the discharge cycles have identical current densities, the discharge curves undergo a rapid and significant voltage drop from 4.5 to 3.5 V, eventually continuing to 0 V. The resistances in Figure 5(b) were determined using these voltage drops. Figure 5(b) shows that the cell containing 30 wt% CA has the highest resistance under a two-stack flow. Figure 5(c) and (d) respectively shows the precise net discharge voltages and powers of each two-stack cell, excluding the voltage drop at the target

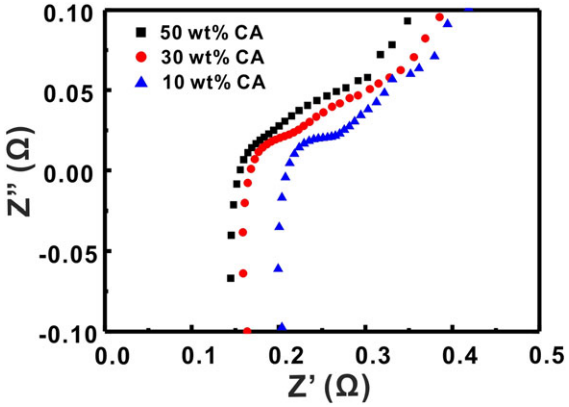

Figure 6. Nyquist plots under different conditions as tested by electrochemical impedance spectroscopy. The tests were conducted with different active material ratios in electrodes under a stack-flow condition (using a slurry electrode with a ratio of 1 to 7 in an activated carbon electrode combined with active materials (AC0830 and Sup-P), with three ratios of the electrolyte in all (1 M TEABF4 in acetonitrile)). Frequency range = 0.01–100,000 Hz; amplitude = 500 mV. CA, conductive additive. [Colour figure can be viewed at wileyonlinelibrary.com]

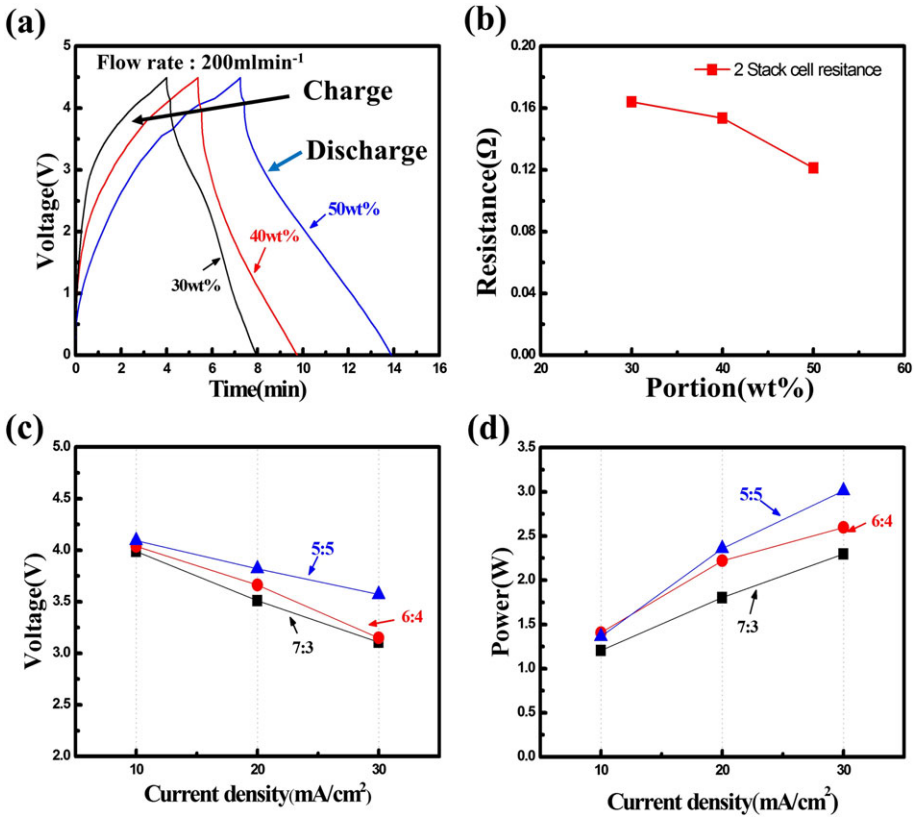

Figure 5. Electrochemical parameters related to the power in a stack-flow condition using galvanostatic charge/discharge methods: (a) charge/discharge curve at 10 mA cm^{-2}, (b) resistance, (c) net discharge voltage, and (d) power, depending of the ratio of the active materials. [Colour figure can be viewed at wileyonlinelibrary.com]

charge voltage of 2.7 V. The cell containing 50 wt% CA exhibits the highest net discharge voltage and power levels at all current densities. The net discharge voltage and power levels in the 50 wt% CA cell at 10, 20, and 30 mA cm^{-2} are 4.1, 3.8, and 3.5 V, and 1.3, 2.4, and 3.1 W, respectively.

Figure 6 shows the electrochemical impedance spectroscopy results, which provide further insight into the complex resistance and diffusion limitations [14]. Figure 6(a) illustrates Nyquist plots of all samples under the two-stack flow condition exhibiting typical capacitive behaviors in the high frequency region and a vertical linear characteristic at a low frequency [11]. The diffusion limitations at low frequencies are depicted as the sloped region in the Nyquist plots, known as the Warburg region. While the 30 wt% two-stack flow cell showed the highest resistance, the 50 wt% two-stack flow cell was less limited in terms of its diffusion characteristics [14].

4. CONCLUSIONS

In this study, we investigated the changes in the electrochemical performance capabilities of CUCap, non-flow, single-flow, and stack-flow cells depending on the portion of the active material. In addition, we observed the networks between a CA and an AC sphere in an effort to devise strategies to overcome the resistance caused by the mass transfer in the flow condition. The performance of the CUcap sample varied with the density of the network. First, while the portion of CA did not largely affect the quantitative parameter or efficiency, the AC ratio was linked to an increase in the performance under the non-flow condition. The slurry electrode containing 20 wt% CA at a slurry ratio of 1 to 7 (electrode to electrolyte (1 M TEABF4 in Acetonitrile)) has the highest energy efficiency value, 82.7% at a current density of 10 mA cm^{-2}. Moreover, we obtained the highest energy density at 10 wt%, 5.8 Wh kg^{-1} at current density of 10 mA cm^{-2}. However, the electrode having a low CA ratio showed a decline of all performance metrics, including the energy efficiency and density. We found that many ion adsorption sites in AC are more helpful than electric 3D networks to improve performance levels in a low resistance condition. Second, in the single-flow condition, the best performance was obtained with 30 wt% CA in a flowable electrode (at a slurry ratio of 1 to 7), resulting in volumetric capacitance and energy efficiency values of 8.7 F mL^{-1} and 50%, respectively. However, 10 wt%, the best performer in the non-flow condition, was found to perform poorly, as noted for every parameter. All values in the tests were smaller than those in the non-flow condition due to the increase in the mass transfer resistance. Furthermore, under the more extreme conditions of a two-stack flow system, we obtained different values. The use of 50 wt% CA in a flowable electrode (at a slurry ratio of 1 to 7) was the most suitable electrode for the CUCap component in a stack system. The 50 wt% electrode demonstrated the highest power of 3.1 W, the highest value among all flowable electrodes tested here. The use of 30 and 40 wt% CA in a flowable electrode (at a slurry ratio of 1 to 7) resulted in similar power values at a low current density (10 mA cm^{-2}), but these samples showed a decline at a high current density due to the high current and enhanced resistance. In summary, we have measured electrochemical performance for each operating condition, specifically, non-flow, flow, and stack flow, along with variation of the amount of CA. According to the results, while having more porous carbon provided advantages in terms of low resistance, having more CA is more favorable for high resistance. Optimizing the CA percentage is an effective route among the many approaches to overcome the resistance limitation under a flow condition. Many ways to improve the electrochemical performance are known, such as adjusting the channel depth and replacing the AC and electrolyte. Therefore, future work should find the most suitable methods to realize an effective energy storage system.

ACKNOWLEDGEMENTS

This work was conducted under the frame work of the Research of Development Program of the Korea Institute of Energy Research (KIER) (B6-2413) and the National Research Foundation (NRF-2011-C1AAA001-0030538).

REFERENCES

1. Weber AZ, Mench MM, Meyers JP, Ross PN, Gostick JT, Liu Q. Redox flow batteries: a review. *Journal of Applied Electrochemistry* 2011; **41**:1137–1164.
2. Yang Z, Zhang J, Kintner-Meyer MC, Lu X, Choi D, Lemmon JP, *et al.* Electrochemical energy storage for green grid. *Chemical Reviews* 2011; **111**:3577–3613.
3. Presser V, Dennison CR, Campos J, Knehr KW, Kumbur EC, Gogotsi Y. The electrochemical flow capacitor: a new concept for rapid energy storage and recovery. *Advanced Energy Materials* 2012; **2**:895–902.
4. Campos JW, Beidaghi M, Hatzell KB, Dennison CR, Musci B, Presser V, *et al.* Investigation of carbon materials for use as a flowable electrode in electrochemical flow capacitors. *Electrochimica Acta* 2013; **98**:123–130.
5. Yeon S-H, Kim D-H, Kim D, Park S-K, Yoon H, Yoo J, *et al.* Cyclic ultracapacitor for fast-charging and scalable energy storage system. *Energy* 2015; **93**:210–219.
6. Stoller MD, Ruoff RS. Best practice methods for determining an electrode material's performance for ultracapacitors. *Energy & Environmental Science* 2010; **3**:1294–1301.

7. Boota M, Hatzell K, Beidaghi M, Dennison C, Kumbur E, Gogotsi Y. Activated carbon spheres as a flowable electrode in electrochemical flow capacitors. *Journal of The Electrochemical Society* 2014; **161**: A1078–A1083.
8. Hassan HM, Abdelsayed V, Abd El Rahman SK, AbouZeid KM, Terner J, El-Shall MS, *et al.* Microwave synthesis of graphene sheets supporting metal nanocrystals in aqueous and organic media. *Journal of Materials Chemistry* 2009; **19**:3832–3837.
9. Simon P, Gogotsi Y. Materials for electrochemical capacitors. *Nature Materials* 2008; **7**:845–854.
10. Zhang C, Hatzell KB, Boota M, Dyatkin B, Beidaghi M, Long D, *et al.* Highly porous carbon spheres for electrochemical capacitors and capacitive flowable suspension electrodes. *Carbon* 2014; **77**:155–164.
11. Yoon H, Kim H-J, Yoo JJ, Yoo C-Y, Park JH, Lee YA, *et al.* Pseudocapacitive slurry electrodes using redox-active quinone for high-performance flow capacitors: an atomic-level understanding of pore texture and capacitance enhancement. *Journal of Materials Chemistry A* 2015; **3**:23323–23332.
12. Porada S, Lee J, Weingarth D, Presser V. Continuous operation of an electrochemical flow capacitor. *Electrochemistry Communications* 2014; **48**:178–181.
13. Hoyt NC, Wainright JS, Savinell RF. Mathematical modeling of electrochemical flow capacitors. *Journal of The Electrochemical Society* 2015; **162**: A652–A657.
14. Boota M, Hatzell K, Alhabeb M, Kumbur E, Gogotsi Y. Graphene-containing flowable electrodes for capacitive energy storage. *Carbon* 2015; **92**:142–149.